Scientific Research Publishing

Study of the Effect of Operating Temperatures (1320 K, 1420 K and 1520 K) on the Vacant Sites of TiN Alloy in B2 Structure at 45%, 50% and 55% N by MEAM Method

Alain S. Dzabana Honguelet[1,2,3]*, Yahnn J. Mighensle Mimboui[1,2,3], Ronolvie Bitho Ondongo[1,2,3], Timothée Nsongo[1,2,4]

[1]Faculty of Science and Technology, Marien Ngouabi University, Brazzaville, Republic of the Congo
[2]Research Group on Physical and Chemical Properties of Materials, Brazzaville, Republic of the Congo
[3]Association Alpha Sciences Beta Technologies, Brazzaville, Republic of the Congo
[4]Center for Geological and Mining Research, Brazzaville, Republic of the Congo
Email: *second_alain@yahoo.fr, mimbouiyahnn@gmail.com

Abstract

In this work, we have studied the vacancy formation energy of TiN alloy of structure B2 of size $10 \times 10 \times 10$ for nitrogen percentages of 45%, 50% and 55% under the influence of temperature at 1320 K, 1420 K and 1520 K using the Modified Embedded Atom Method MEAM under the calculation code LAMMPS version 2020. This study has enabled us to understand the behavior of the TiN alloy under different nitrogen percentages in terms of total energy, vacancy formation energy, crystalline parameter, occupancy rate and order parameter. For total energy, we have shown that as temperature increases, total energy decreases, making it easier to obtain TiN at higher temperatures; reaching the value of -7344.9169 eV for the 55% nitrogen structure for the temperature of 1420 K. For the energy of formation, we have shown that the compounds obtained at 1320 K and 1520 K have a more considerable energy of formation than that obtained at 1420 K. The study of fractions and the order parameter showed us that the structure of TiN with 55% nitrogen is less likely, as the composition obtained is at most 53.35%.

Keywords

1. Introduction

Titanium nitride is a chemical compound with the formula TiN. It is an ultra-hard, corrosion-resistant ceramic. It is commonly used as a coating for titanium alloys and components made of steel, carbides and aluminum, to improve their surface properties [1] [2].

The first area of application for TiN deposits is mechanical engineering, and this remains an important field of application, the aim being to increase the service life and working performance of cutting and forming tools. These tools are generally coated with a protective layer of TiN to improve wear and abrasion resistance [3], hardness [4], chemical stability [5], coefficient of friction [6] and thermal conductivity for faster heat dissipation.

Its excellent electrical conductivity, adhesion and chemical stability make titanium nitride an ideal material [7]. These properties are also exploited in the design of other electronic devices, such as gate electrodes in MOS transistors, low-barrier Schottky diodes and many other applications where silicon is used as a substrate [8].

Another example is the use of titanium nitride as a gas diffusion barrier in ultra-high vacuum chambers, where TiN deposits reduce hydrogen permeability and thus improve the ultimate vacuum [9].

Finally, the optical properties of TiN are exploited not only for selective light transmission [10], but also for aesthetic and decorative reasons. Since stoichiometric titanium nitride is golden yellow in color, it is widely used in jewelry, where it replaces gold [11]. Its high resistance to scratches and corrosion are further asset [12].

Antoine PARIS has worked on the study of Phase Transformations in TiN-based alloys with low silicon alloys [13]. The aim of his work was to increase our knowledge of silicide precipitation in titanium aluminides, so as to be in a position to propose a metallurgical route optimizing this structural transformation and, if necessary, improving the mechanical properties of these alloys. To this end, he has contributed to developing knowledge of phase equilibria in the Ti-N-Si ternary system. He then characterized the structural modifications of four alloy compositions, during solidification and then during solution heat treatment and precipitation.

Sandrine AMELIO led studies on the microstructural evolution of a TiN-based alloy [14]. This study investigated the microstructural evolution of a TiN-based intermetallic alloy under dynamic compressive loading, as well as its performance under isothermal heat treatment. The TiN-based alloy studied is characterized by good mechanical properties at high temperatures and low density.

Professor Timothée NSONGO has studied the order-disorder transformation of the binary TiN alloy system by numerical simulation using the EAM inserted atom method [15]. The aim of this thesis was mainly to determine the influence of lattice constant, composition on the type of order-disorder transformation and order processes in alloys.

Mohamed BENHAMIDA has worked on the structural, elastic and electronic properties of transition metal nitride alloys [16]. He studied the structural, electronic and mechanical properties of transition metal nitrides using DFT density functional theory and compared them with experimental results.

This work takes the same approach as the previously cited authors, but our study is much more particular in that it investigates the structure of the TiN alloy by computer simulation using the MEAM potential, which is an appropriate potential for the study of metal alloys. In addition, we focus on the study of vacant sites in order to determine the most stable structure of the TiN alloy under the influence of temperature.

2. Methodology

The aim of this work is to study the TiN alloy system in B2 structure at different temperatures (1320 K, 1420 K and 1520 K) as a function of different atomic percentages of nitrogen (45%, 50% and 55%) in order to determine the influence of atomic percentage composition and temperature on the lattice parameter and to determine its vacation formation energy and temperature in order to find out at which percentage and temperature the TiN alloy is stable.

To do this, we worked with a $10 \times 10 \times 10$ system of the TiN alloy consisting of a total of 2000 atoms, simulated using the LAMMPS calculation code and the MEAM (Modified Embedded Atom Method) interatomic potential.

A vacancy was created in the middle of the structure. The energy of the structure before and after the creation of the vacancy was used to determine the energy of formation of the vacancy.

In addition to calculating the vacancy formation energy, several different analysis methods were used to determine how vacancy, temperature and alloying would affect the overall stability of the atomic structure.

We ran a simulation under the LAMMPS code version 2020 with the executable lmp_mpi, under the Windows operating system, using the MEAM potentials found in the database at https://www.ctcms.nist.gov.

The MEAM potentials of titanium, nitrogen and titanium nitride used in this work were developed respectively by Y.-M. Kim, B.-J. Lee, and M.I. Baskes (2006) and Y. M. Kim and B. J. Lee, (2008), whose parameters are aligned in the following Table 1 and Table 2 [17] [18] [19] [20] [21].

These potentials have been used to calculate cohesive energies under different structures Lammps calculation code and MPC4 software.

Here are the different crystalline structures of TiN alloy (Figure 1).

Table 1. Additional titanium and nitrogen parameters.

elt	atwt	alat	β_0	β_1	β_2	β_3	t_0	t_1	t_2	t_3	esub	asub	α	Z	lat	ibar	rozero
Ti	47.88	2.92	2.7	1.0	3.0	1.0	1.0	6.8	−2.0	−12.0	4.87	0.66	4.71	12	hcp	3.0	1.0
N	14.00	1.10	2.75	4.0	4.0	4.0	1.0	0.05	1.0	0.00	4.88	1.80	5.96	1	dim	3.0	18

Table 2. MEAM parameters for Ti, Al and TiN.

Symbols	Ti	N	TiN
rc (A˚)	4.8	4.6	4.6
delr	0.1	0.1	0.1
augt1	0	1	0
erose_form	2	0	2
ialloy	2	2	2
zbl(1, 1)	0	1	0
nn2(1, 1)	1	0	1
rho0(1)	1.00	1.00	18
Ec(1, 1)	4.870	4.88	6.615
re(1, 1)	2.920	1.10	2.121
alpha(1, 1)	4.719	4.330	5.092
repuls(1, 1)	0.00	0.00	0.00
attrac(1, 1)	0.00	0.00	0.00
Cmin(1, 1, 1)	1.00	2.00	0.16
Cmax(1, 1, 1)	1.44	2.80	2.80
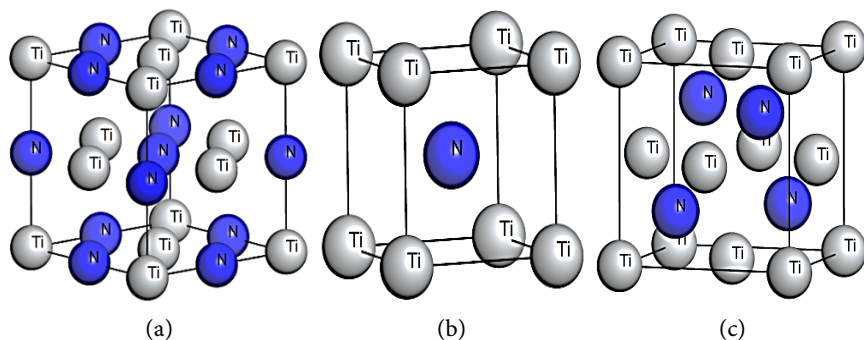
Figure 1. Different crystallographic structures of TiN: (a) B1 (NaCl), (b) B2 (CsCl), (c) B3 (ZnS).

2.1. Molecular Dynamics

Molecular Dynamics is a formidable tool for investigating matter at the atomic scale. It involves numerically simulating the evolution of a system of particles as a function of time, with the aim of predicting and understanding experimental results. It can reveal structural arrangements or dynamic phenomena that are still inaccessible to current experimental means of observation (NMR, Atom Probe Tomography), especially in the case of amorphous materials such as glasses. This move into the digital world requires a discretization of time to solve the Newtonian equations governing the motion of each particle. The principle of Molecular Dynamics is then to integrate these discretized equations, under various physical constraints, using a variety of algorithms.

The potentials used must first and foremost account for known properties, in

order to be able to predict those that are not, or to explain a phenomenon that is still poorly understood. These methods and algorithms are finally applied to the modeling of silica materials, in particular glasses, where certain properties and experimental behaviors are reproduced with acuity [22] [23].

2.1.1. Principle of Molecular Dynamics

Classical molecular dynamics (DM) is based on Newtonian mechanics: the properties of a set of atoms or particles are determined by studying the trajectory of each particle over time. To do this, the laws of classical mechanics are applied to atoms, which are treated as point masses. The classical equations of motion are thus solved simultaneously for all the atoms in a system [24] [25]:

$$\boldsymbol{f}_i = m_i \boldsymbol{a}_i \tag{1}$$

where $\boldsymbol{f}_i$ is the sum of the forces acting on atom *i*, m_i its mass and $\boldsymbol{a}_i$ its acceleration.

The integration of the equations of motion has to be done numerically; choosing a finite time step δt and approximating the differential equations by finite difference equations. From these calculations, the computer predicts the new positions, velocities and forces of all the particles at time $t + \delta t$. In this way, we can trace the behavior of a material: for example, the movement and rearrangement of atoms/defects.

The input data for a molecular dynamics' calculation are therefore:

➢ A set of atoms, representing in our case the system to be studied;
➢ Interatomic potentials, the determination of which requires prior study;
➢ Eventually, a series of constraints imposed by the external environment (pressure, temperature, etc.).

2.1.2. Integration Algorithms for Newton's Equations

The basic numerical method for solving the equations of motion corresponds to performing a Taylor series expansion to 2nd order of position *x* around date *t*, *i.e.* to $t \pm \delta t$ (with δt small):

$$\begin{cases} x(t+\delta t) = x(t) + \delta t \dfrac{\mathrm{d}x}{\mathrm{d}t} + \dfrac{1}{2}\delta t^2 \dfrac{\mathrm{d}^2 x}{\mathrm{d}t^2} \\ x(t-\delta t) = x(t) - \delta t \dfrac{\mathrm{d}x}{\mathrm{d}t} + \dfrac{1}{2}\delta t^2 \dfrac{\mathrm{d}^2 x}{\mathrm{d}t^2} \end{cases} \tag{2}$$

By adding and grouping the terms, we obtain:

$$\frac{\mathrm{d}^2 x}{\mathrm{d}t^2} = \frac{1}{\delta t^2}\left[x(t+\delta t) - 2x(t) + x(t-\delta t) \right] \tag{3}$$

We discretize time using a time step δt (of the order of femto seconds in Molecular Dynamics). At iteration *n*, the date is expressed by $t_n = n\delta t$, the position vector by x_i^n the velocity vector by v_i^n and the force vector by F_i^n. After this discretization and digitization, the previous equation becomes, for the date $t_{n+1} = t_n + \delta t$:

$$m_i \frac{1}{\delta t^2} \left(x_i^{n+1} - 2x_i^n + x_i^{n-1} \right) = F_i^n \tag{4}$$

In the same way, but subtracting the terms this time, we obtain the velocity expression:

$$v_i^n = \frac{x(t + \delta t) - x(t - \delta t)}{2\delta t} = \frac{x_i^{n+1} - x_i^{n-1}}{2\delta t} \tag{5}$$

This is the standard form of the Störmer-Verlet method for integrating Newton's equations:

$$\begin{cases} x_i^{n+1} = 2x_i^n - x_i^{n-1} + \frac{\delta t^2}{m_i} F_i^n \\ v_i^n = \frac{x_i^{n+1} - x_i^{n-1}}{2\delta t} \end{cases} \tag{6}$$

2.2. Interaction Potentials and the MEAM Method

To model a material, we select and parameterize an interatomic potential, from which we derive the forces interacting between the different particles present in the simulation box. This is usually an effective potential. Its parameterization is such that, through its effects, the model reproduces known properties of the simulated material (crystalline structures, elastic properties, X-ray diffraction pattern, infrared spectrum, NMR, etc.). A correctly parameterized interaction potential is crucial for predicting or interpreting as yet unexplained properties of the material being modeled. This parameterization is often tedious, which is why some authors publish their parameters, enabling a large number of modelers to use them, which also offers a consistent common basis for studying and comparing materials [26] [27]. For modeling silica-based glasses, there are, for example, the MEAM potential and Buckingham potential described below and used in this dissertation work.

MEAM Formalism and MEAM Potential

Interatomic potentials are of vital importance for simulations that model the properties of materials. The basis for these potentials is Density Function Theory (DFT), which postulates that energy is a function of electron density. By knowing the electron density of an entire system, we can determine the potential energy of a system:

$$E\left[\rho(r)\right] = Ts\left[\rho(r)\right] + J\left[\rho(r)\right] + E_{xc}\left[\rho(r)\right] + E_{ext}\left[\rho(r)\right] + E_{ii}\left[\rho(r)\right] \tag{7}$$

where E is the total energy, Ts is the kinetic energy of the single particle, J is the Hartree electron-electron energy, E_{xc} is the exchange correlation function, E_{ext} is the electron-ion coulombic interaction, and E_{ii} is the ion-ion energy.

On this basis, the Embedded Atom Method (EAM) was created on the assumption that an atom can be embedded in a homogeneous electron gas and that the change in potential energy is a function of the electron density of the embedded atom, which can be approximated by an embedding function. In a

crystal, however, the electron density is not homogeneous, so the EAM potential replaces the background electron density with the electron densities of individual atoms, and supplements the embedding energy with a repulsive pair potential to represent the core-core interactions of the atoms.

However, EAM does not do an excellent job of simulating materials with significant directional binding, which includes most metals. In order to simulate metals correctly, the modified embedded atom method was created, which allows the background electron density to depend on the local environment instead of assuming a linear superposition.

In the MEAM formalism, we consider a set of atoms forming a cluster. Each atom is immersed in the electron density created by the other atoms. The total energy depends on two factors: the immersion potential and the pair interaction potential:

$$E = \sum_i F_i\left(\overline{\rho}_i\right) + \frac{1}{2}\sum_{j \neq 1} \phi_{ij}\left(R_{ij}\right) \tag{8}$$

For an atom i, F_i is the immersion potential, $\overline{\rho}_i$ is the fundamental electron density. $\phi_{ij}\left(R_{ij}\right)$ is the pair interaction potential between two atoms i and j, at distance R_{ij}.

Immersion potential is calculated as follows:

$$F_i\left(\overline{\rho}_i\right) = AE_c\frac{\overline{\rho}_i}{\rho_0}\ln\left(\frac{\overline{\rho}_i}{\rho_0}\right) \tag{9}$$

where

A is a parameter that can be adjusted according to experimental data;

E_c is the sublimation energy:

ρ_0 the electron density in the reference structure;

$\overline{\rho}_i$ the electron density in the real structure.

In MEAM1, the consideration of interactions in the reference structure is limited to the first neighborhood. Under these conditions, atomic positions and bond directions are fixed. The immersion potential depends only on the distance to the first neighbor and the number of first neighbors. Consequently, the energy of an atom can be written as a function of R as follows:

$$E^u\left(R\right) = F\left[\overline{\rho}_i^0\left(R\right)\right] + \frac{Z_1}{2}\phi\left(R\right) \tag{10}$$

where Z_1 is the number of the atom's first neighbors.

By calculating $E^u\left(R\right)$ from Rose's equation of state, we can derive the expression for the interaction potential of the pairs as follows:

$$\phi\left(R\right) = \frac{2}{Z_1}\left[E^u\left(R\right) - F\left[\overline{\rho}_i^0\left(R\right)\right]\right] \tag{11}$$

In MEAM2, we consider second-neighbor interactions in the reference structure, and this can be achieved by adding a screen parameter S. From this, the energy of an atom in a reference structure can then be written:

$$E^{u}(R) = F\left[\bar{\rho}_i^0(R)\right] + \frac{Z_1}{2}\phi(R) + \frac{Z_2 S}{2}\phi(aR) \tag{12}$$

where

Z_1 is the number of first neighbors in the reference structure;

Z_2 is the number of second neighbors in the reference structure;

a is the ratio of the distances of second and first neighbors $a = R_2/R_1$;

S is the screen function for a given reference structure, the screen factor *S* is constant.

The above equation can be written as:

$$E^{u}(R) = F\left[\bar{\rho}_i^0(R)\right] + \frac{Z_1}{2}\psi(R) \tag{13}$$

with

$$\psi(R) = \phi(R) + \frac{Z_2 S}{Z_1}\phi(aR) \tag{14}$$

From the value $\psi(R)$ the pair interaction potential is iteratively calculated using the following formula:

$$\phi(R) = \psi(R) + \sum_{n=1}(-1)^n\left(\frac{Z_2 S}{Z_1}\right)^n\psi(a^n R) \tag{15}$$

The main difference between the potential energy equation for EAM and MEAM is the inclusion of *S*, which reflects the shielding effect.

For a MEAM interatomic potential that describes the relationship for alloys with two or more components, each of the components needs 13 individual adjustable parameters. In addition, each binary interaction requires at least 14 adjustable parameters.

2.3. Vacancy Formation Energy

To calculate the vacancy formation energy, a single vacancy was introduced into a perfect lattice with equilibrium lattice constants and structural relaxation of atomic positions. Only isolated, non-interacting defects were taken into account when calculating defect formation energy.

In general, the energy of formation of a vacancy in a homogeneous bulk crystal that does not change phase can be described by:

$$E_{fv} = E_{(n-1)} - \frac{n-1}{n}E_n \tag{16}$$

$E_{(n-1)}$ is the total energy of an atomic supercell containing a vacancy, while E_n is the total energy of this supercell before the vacancy was created. In this research, the energy of vacancy formation was calculated by taking averages in two different ways illustrated in the results section.

In this research, vacancy formation energy was calculated by taking averages in two different ways. In the first case, the total energy of the last 10,000 MD

steps of each stage was averaged before integration.

The energy per atom of each step is then averaged. For the error, the variance of the energy per atom of each step was calculated. In the final method, the difference in total energy was calculated for each individual step.

Next, we calculate the total energy required to create the vacancy:

$$E_{total} = \sum E_{fv} \tag{17}$$

3. Results

In this section, we present the results obtained for the total energy before and after the creation of the vacancy, the crystalline parameter under the effect of temperature, the occupancy rate and the short-range order parameter—all these physical quantities under the effect of the operational temperatures 1320 K, 1420 K and 1520 K.

3.1. Total Energy and Energy of Vacancy Formation

As we saw in the method section, vacancy formation energy was calculated using two different methods; the first and second methods used the total energy of the atomic structure.

As a result, these two methods provide incredibly similar results, which are also of the same order of magnitude as previous literature on the vacancy formation energy of titanium.

The results for total energy before and after vacancy creation are shown in Table 2 and Table 3.

3.1.1. Total Energy

We present here the results of methods 1 and 2 on total energy in Table 3 and Table 4. We note that total energy decreases with temperature and also with the percentage of nitrogen, regardless of the method used.

This table shows that:

➤ For a given percentage, as the temperature increases, the energy of formation decreases, making it easier to obtain TiN at higher temperatures;

➤ For a constant temperature, the energy of formation increases with the percentage of nitrogen.

Table 3. Total energy.

Temperature (K)	Total energy (method 1)		
	%N		
	45	50	55
1320	−8324.8537	−7863.1167	−7356.1984
1420	−8354.4795	−7872.7571	−7344.9169
1520	−8330.5641	−7749.336	−7442.5377

Table 4. Formation energy (method 2).

Temperature (K)	Training energy								
	%N								
	45			50			55		
Energy	Ei	Ef	E_f	Ei	Ef	E_f	Ei	Ef	E_f
1320	−8324.853	−6791.218	1529.472	−7863.116	−6411.154	1448.030	−7356.198	−5568.170	1784.349
1420	−8354.479	−6649.229	1701.072	−7872.757	−6113.016	1755.804	−−7344.916	−5808.660	1532.583
1520	−8330.564	−6521.081	1805.317	−7749.335	−6104.785	1640.675	−7442.537	−5375.422	2063.394

3.1.2. Total Energy and Formation Energy

The second method enabled us to evaluate the energy of formation simultaneously by calculating the initial and final energies before and after the creation of the vacancy, randomly removing either the titanium or nitrogen atom. The results are shown in Table 4.

These results from the second method are consistent with the results from the first method. The formation energy values obtained interpret the possibility of obtaining the structure at any temperature.

Figure 2 shows a double monotonicity: one part decreasing, the other increasing.

➢ Decreasing part; ranging from 44% to 50%, the dominant compound is likely to form at 1420 K ahead of that obtained at 1520 K;

➢ For the decreasing part: from 50% to 55%, the compounds obtained at 1320 K and 1520 K have a more considerable formation energy than that obtained at 1420 K.

1520 K is an excellent temperature for TiN production.

3.1.3. Mesh Parameter Evolution

During the course of this work, we also monitored the evolution of the mesh parameter of the $10 \times 10 \times 10$ structure of the TiN alloy as a function of percentage and temperature. The results are shown in Table 5.

These results led to Figure 3 below:

➢ The behavior of the evolution of the mesh parameter is remarkable for the structure obtained at 1320 K, first increasing between 45% and 50% N then decreasing thereafter;

➢ The structures obtained at 1420 K and 1520 K show the same behavior, decreasing as the percentage of nitrogen increases.

However, although different in some cases, it is remarkable to see that all the structures, whatever their operating temperature, have the same mesh parameter around 1520 K.

3.1.4. Atomic Fraction of Nitrogen

We monitored the composition of TiN as a function of temperature and percentage of nitrogen, and the results are shown in Table 6 below.
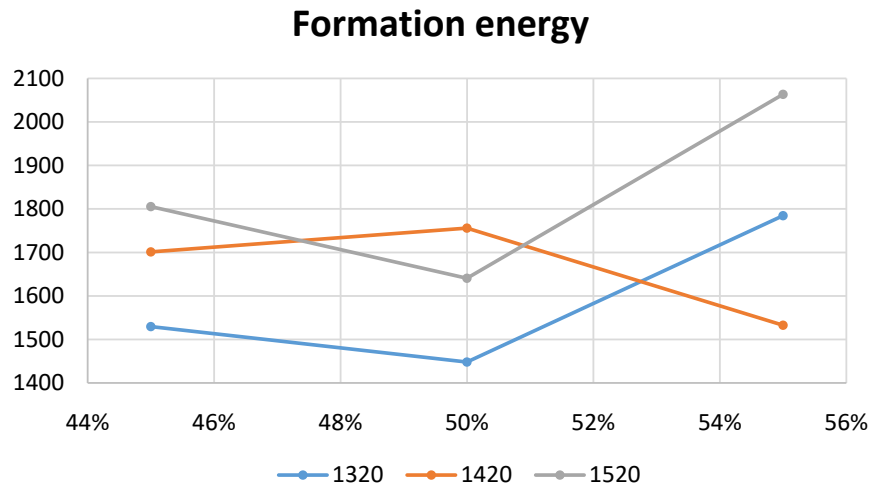
Formation energy

Figure 2. Energy of formation by percentage of nitrogen.

Mesh parameter evolution
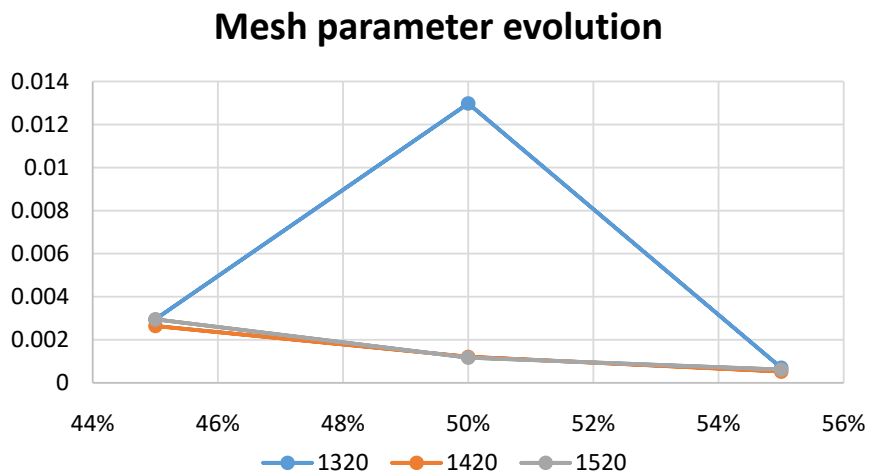
Figure 3. Mesh parameter variation vs %N.

Table 5. Formation energy.

| Temperature (K)	Temperature and parameter								
	%N								
	45			50			55		
	Init.	Final	Diff.	Init.	Final	Diff.	Init.	Final	Diff.
1320	32.7	32.7029	0.0029	32.7	32.7012	0.0129	32.7	32.7007	0.0007
1420	32.7	32.7026	0.0026	32.7	32.7012	0.0012	32.7	32.7005	0.0005
1520	32.7	32.7029	0.0029	32.7	32.7011	0.0011	32.7	32.7006	0.0006

In most cases, we can see from **Table 6** that the filling ratio is close to the percentages of nitrogen in the titanium alloy.

Figure 4 shows us that:

- Whatever the temperature, the percentage takes precedence over the evolution of the structure;

Table 6. Fraction by percentage of nitrogen.

Temperature(K)	Training energy		
	%N		
	45	50	55
1320	0.449	0.492	0.533
1420	0.449	0.4925	0.5335
1520	0.4485	0.4925	0.5335
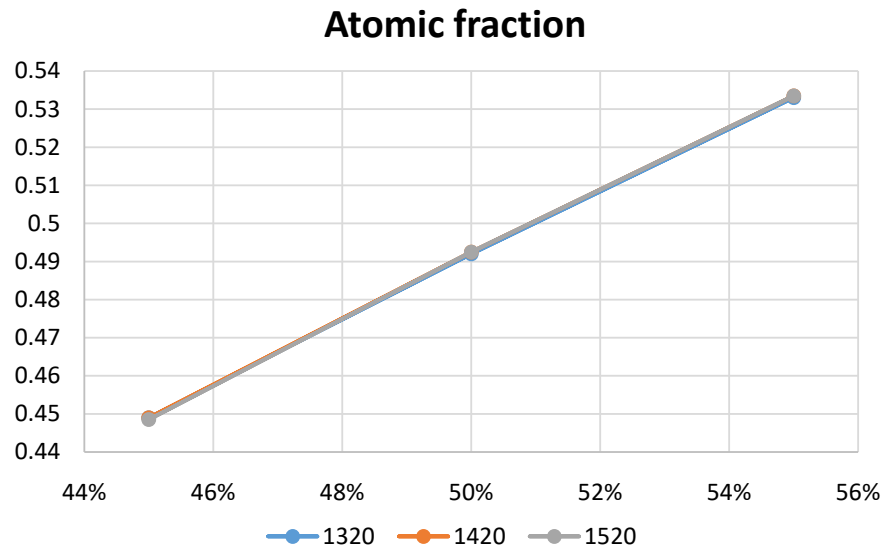
Figure 4. Atomic fraction as a function of %N.

- The structures obtained with 45% and 50% nitrogen have a high probability of being formed with the same parameters, as their compositions are close to the proposed percentages;
- The TiN structure with 55% nitrogen is less likely, as the composition obtained is at most 53.35%.

3.1.5. Order Parameter

The filling ratio is closely linked to the configurations and therefore to the order parameter we wanted to observe in order to understand the behavior of the titanium alloy structure for different nitrogen percentages.

Thus, for the SRO parameter, for a system with an equal number of atom types

A and B, a perfectly ordered network has $\sigma = 1$, a phase-separated system has $\sigma = -1$, and a totally random solid solution has $\sigma = 0$.

Although it is a simple quantified representation of a potentially complex order, the order parameter is generally interpreted in terms of three values: negative, zero and positive (**Table 7**).

Figure 5 shows that TiN structures obtained at 1320 K have the highest probability of being formed, whatever the percentage used.

Table 7. Order parameter and formation energy.

Temperature (K)	Order parameter-formation energy					
	%N					
	45	Ef	50	Ef	55	Ef
1320	0.00181	1529.4726	0.01574	1448.0305	0.036402	1784.3494
1420	0.00181	1701.0728	0.01477	1755.8042	0.035369	1532.5835
1520	0.00271	1805.3176	0.01477	1640.6757	0.03536	2063.3942
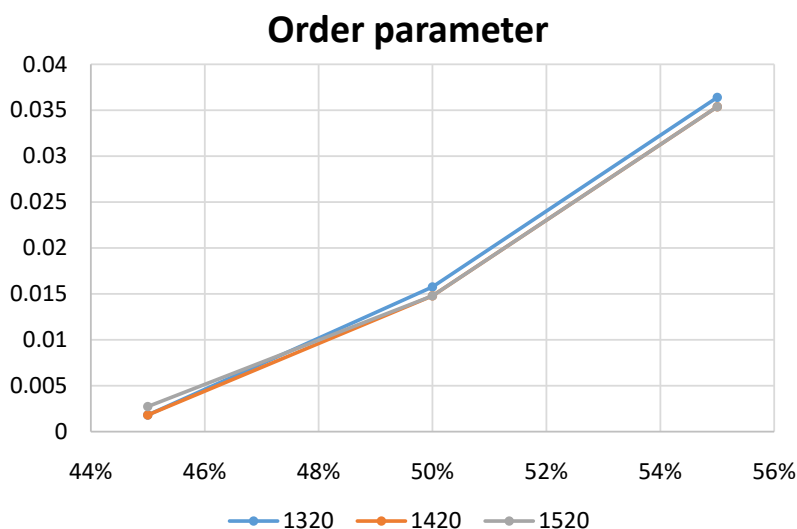
Figure 5. Order parameter.

4. Conclusions

In this work, we used the MEAM potential of TiN to track the structural behavior of the B2-type cubic-centered phase TiN alloy in terms of the formation energy of the randomly created central gap, at operational temperatures 1320 K, 1420 K and 1520 K.

This study highlighted the consequences of the central gap on the probability of obtaining a new TiN phase.

The energy of formation shows us that it is more practical to obtain a TiN alloy at high temperature.

The compounds obtained at 1320 K are more stable than the others; this is confirmed by the order parameter.

The best stoichiometric composition of TiN is in the range of 44.9% to 53.35% nitrogen for it to be stable in B1 structure.

Acknowledgements

Conflicts of Interest

The authors declare no conflicts of interest regarding the publication of this paper.

References

[1] Pierson, H.O. (1996) Handbook of Refractory Carbides and Nitrides. Properties, Characteristics, Processing and Applications. Noyes Publications, Park Ridge.

[2] Centre Technique des Industries Mécaniques (CETIM) (1987) Manuel des traitements de surface à l'usage des bureaux d'étude. CETIM, Paris.

[3] Bauer, A.D., Herranen, M., Ljungcrantz, H., Carlsson, J.-O. and Sundgren, J.-E. (1997) Corrosion Behaviour of Monocrystalline Titanium Nitride. *Surface and Coatings Technology*, **91**, 208-214.
http://www.sciencedirect.com/science/article/pii/S0257897297000030

[4] Mäntylä, T.A., Helevirta, P.J., Lepistö, T.T. and Siitonen, P.T. (1985) Corrosion Behaviour and Protective Quality of TiN Coatings. *Thin Solid Films*, **126**, 275-281.
https://doi.org/10.1016/0040-6090(85)90321-9

[5] Shreir, L.L. (1976) Corrosion. Vol. 1, Newnes, Butterworths, London.

[6] Jehn, H.A. (2000) Improvement of the Corrosion Resistance of PVD Hard Coating-Substrate Systems. *Surface and Coatings Technology*, **125**, 212-217.
https://doi.org/10.1016/S0257-8972(99)00551-4

[7] Mansfeld, F. (1971) Area Relationships in Galvanic Corrosion. *Corrosion*, **27**, 436-442. https://doi.org/10.5006/0010-9312-27.10.436

[8] Carradot, M., Ter-Ovanessian, B. and Normand, B. (2016) Galvanic Coupling Criticality of Passive Stainless Steel Coated by Noble Materials: Role of Porosity Morphology and Distribution.

[9] Massiani, Y., Medjahed, A., Crousier, J.P., Gravier, P. and Rebatel, I. (1991) Corrosion of Sputtered Titanium Nitride Films Deposited on Iron and Stainless Steel. *Surface and Coatings Technology*, **45**, 115-120.
https://doi.org/10.1016/0257-8972(91)90213-G

[10] Laugier, M.T. (1986) Adhesion of TiC and TiN Coatings Prepared by Chemical Vapour Deposition on WC-Co-Based Cemented Carbides. *Journal of Materials Science*, **21**, 2269-2272. https://doi.org/10.1007/BF01114266

[11] Braccini, M. and Dupeux, M. (2013) Mechanics of Solid Interfaces. John Wiley & Sons, Hoboken. https://doi.org/10.1002/9781118561669

[12] Toscan, F. (2004) Joint Optimization of Oxide Layer Adhesion and Thermal Oxidation Kinetics on Stainless Steels.

[13] Paris, A. (2015) Study of Phase Transformations in TiN Base Alloys with Low Silicon Alloying. Universite de Lorraine, Nancy.

[14] Amelio, S. (2005) Microstructural Evolution of a TiN-Based Alloy: Mechanical Loading by Dynamic Compression and Thermal Stability. Institut National Polytechnique de Lorraine, Nancy.

[15] Nsongo, T. (2001) Computer Simulation of Order-Disorder Transformation for TiN Binary System. University of Science and Technology Beijing, Beijing.

[16] Benhamida, M. (2014) Structural, Elastic and Electronic Properties of Transition Metal Nitride Alloys. University of Setif 1, Stif.

[17] Kim, Y.-M., Lee, B.-J. and Baskes, M.I. (2006) Modified Embedded-Atom Method

Interatomic Potentials for Ti and Zr. *Physical Review B*, **74**, Article ID: 014101. https://doi.org/10.1103/PhysRevB.74.014101

[18] Kim, Y.-M., and Lee, B.-J. (2008) Modified Embedded-Atom Method Interatomic Potentials for the Ti-C and Ti-N Binary Systems. *Acta Materialia*, **56**, 3481-3489. https://doi.org/10.1016/j.actamat.2008.03.027

[19] Yoo, M.H., Daw, M.S. and Baskes, M.I. (1989) Atomistic Simulation of Materials: Beyond Pair Potentials. In Vitek, V., and Srolovitz, D.J., Eds., Plenum, New York, 401. https://doi.org/10.1007/978-1-4684-5703-2_41

[20] LAMMPS and MEAM Parameters Descriptions. http://lammps.sandia.gov/doc/pair_meam.html

[21] Baskes, M.I., Nelson, J.S. and Wright, A.F. (1989) Semiempirical Modified Embedded-Atom Potentials for Silicon and Germanium. *Physical Review B*, **40**, 6085-6100. https://doi.org/10.1103/PhysRevB.40.6085

[22] Allen, M.P. (2004) Introduction to Molecular Dynamics Simulation. In: Attig, N., Binder, K., Grubmuller, H. and Kremer, K., Eds., *Computational Soft Matter: From Synthetic Polymers to Proteins, NIC Series*, Vol. 23, John von Neumann Institute for Computing, Julich, 1-28.

[23] Allen, M.P. and Tildesley, D.J. (1989) Computer Simulation of Liquids. Oxford University Press, Oxford.

[24] Becquart, C. and Perez, M. (2015) Molecular Dynamics Applied to Materials. https://www.techniques-ingenieur.fr/

[25] Qu, M.Y. (2022) Molecular Modeling and Molecular Dynamics Simulation Studies on the Selective Binding Mechanism of MTHFD2 Inhibitors. *Computational Molecular Bioscience*, **12**, 1-11. https://doi.org/10.4236/cmb.2022.121001

[26] Daw, M.S., Foiles, S.M. and Baskes, M.I. (1993) The Embedded-Atom Method: A Review of Theory and Applications. *Materials Science Reports*, **9**, 251-310. https://doi.org/10.1016/0920-2307(93)9s0001-U

[27] Dongare, A.M. and Zhigilei, L.V. (2005) A New Embedded Atom Method Potential for Atomic-Scale Modeling of Metal-Silicon Systems. *Proceedings of the International Conference on Computational and Experimental Engineering and Sciences*, Chennai, 1-6 December 2005, 2552-2559.